THE EUROPEAN PHYSICAL JOURNAL D

Performance improvement of nitride semiconductor-based deep-ultraviolet laser diodes with superlattice cladding layers

Yuan Xu[1], Pengfei Zhang[1], Aoxiang Zhang[1], Mengshuang Yin[1], Fang Wang[1,2,3,4,a], Juin. J. Liou[1,2,4], and Yuhuai Liu[1,2,3,4,b]

[1] National Center for International Joint Research of Electronic Materials and Systems, School of Information Engineering, Zhengzhou University, Zhengzhou 450001, China
[2] Research Institute of Sensors, Zhengzhou University, Zhengzhou 450001, China
[3] Zhengzhou Way Do Electronics Technology Co. Ltd., Zhengzhou 450001, China
[4] Industrial Technology Research Institute Co. Ltd., Zhengzhou University, Zhengzhou 450001, China

Abstract. A deep-ultraviolet (DUV) laser diode (LD) consisting of specifically designed cladding layers involving superlattice nitride alloy has been proposed. Simulation studies of different cladding layers were carried out using Crosslight software. It was found that the proposed structure effectively suppresses the leakage of the optical field from the active region and the optical confinement coefficient is 1.45 times higher than that of the conventional structure. The proposed structure has a significant increase in laser power with a low threshold current. Moreover, the introduction of novel cladding layer suppresses the electron and hole leakage from the multiple quantum well (MQW) region, which provides an attractive solution for increasing the stimulated recombination rate in the MQW region leading to the improvement in the performance of the DUV LD.

1 Introduction

AlGaN-based ultraviolet emitters (light-emitting diode, laser diode) have attracted widespread attention due to their application in water purification, bio-chemical sensing, surfaces disinfection, and medical equipment sterilization [1]. Since the emergence of humans in nature, humans have coexisted with a variety of bacteria and diseases. The recent global pandemic caused by the Severe Acute Respiratory Syndrome Coronavirus (SARS-CoV-2) has not only posed a great risk to human life but also caused damage to the world economy. Therefore, the use of harmless ultraviolet-C (UVC) light technology to inactivate viruses and bacteria is inevitable in order to solve global problems such as infectious diseases [2–4]. According to the investigation of the International Ultraviolet Association (IUVA), DUV light sources emitting wavelengths located at 250–280 nm have an inactivating effect on SARS-CoV2. Although light-emitting diodes (LEDs) can also perform some of these functions, their large size, high cost, and low efficiency limit their widespread

use in the deep-ultraviolet band [5]. The relative semiconductor laser diode has the advantages of small size, low cost, high conversion efficiency, high power, and easy integration [6]. Due to its excellent energy band tuning capability, ternary $Al_xGa_{1-x}N$ alloys with medium or high aluminum components are among the most promising optoelectronic materials in the deep-ultraviolet band [7]. Nevertheless, the realization of highly efficient AlGaN-based laser diodes in the UV-C range still faces many challenges. For instance, the high dislocation density and dot defects in the device during the growth process will lead to high electron leakage and inhibit the radiative recombination in the active region, the high activation energy of the Mg dopant in p-type AlGaN weakens the conductivity in the p-type region and the hole injection efficiency in the MQW region [8–10]. In addition, mobility of electrons is higher than that of holes, so a large number of electrons in the active region will leak into the p region [11]. The intense polarization electric field of AlGaN material with a high Al component results in the Quantum-confined Stark effect (QCSE), which leads to the poor overlap of electron and hole wave functions and affects the optical gain and laser emission of LD [12]. The existence of these problems limits the improvement of the optoelectronic performance of DUV LD.

[a] e-mail: iefwang@zzu.edu.cn (corresponding author)
[b] e-mail: ieyhliu@zzu.edu.cn (corresponding author)

Many efforts have been made to develop efficient AlGaN DUV emitters. For instance, Preparation of high quality AlGaN layers using freestanding AlN substrates [13]. Late Akasaki et al. have reduce threshold current density by improving optical confinement factor and carrier injection efficiency of AlGaN ultraviolet semiconductor lasers [14, 15]. Various electron-blocking layers have also been introduced to reduce electron leakage and improve hole injection efficiency [16–18]. However, little research has been done on the cladding layers of LD.

In this paper, we have proposed novel cladding layers containing superlattice nitride alloy and compared the performances with conventional structure with proper numerical analysis. The light intensity, refractive index, and stimulated recombination rate are simulated, and subsequently optoelectronic performances are rigorously investigated. Simulation results prove that the introduction of superlattice cladding layers can effectively improve the performance of LD.

2 Device structure

Three different types of DUV LD structures assumed on (0001)sapphire substrate are considered in this paper for design, as shown in Fig. 1. The first of these structures is the conventional DUV LD, which is considered to be the reference (LD1). It consists of a 0.5 μm thick Si-doped $Al_{0.78}Ga_{0.22}$N cladding layer (n-CL), 0.1 μm thick Si-doped $Al_{0.75}Ga_{0.25}$N
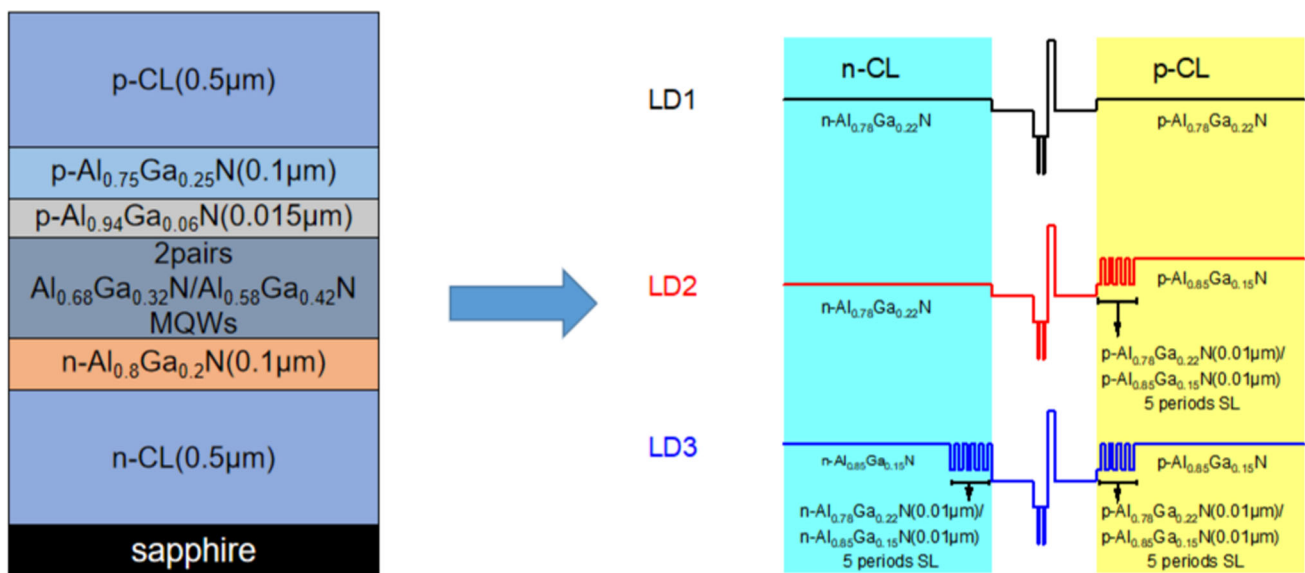

Fig. 1 Schematic of proposed two DUV LD structures along with reference structure

Fig. 2 The simulated Landsberg model gain of DUV LDs. It is weighted gain, which is higher in the MQW region, for emission spectral implementation. The gain reaches a maximum at (267 nm) 0.267 μm when all devices have the same MQW size and composition, so the same model gain is obtained in the MQW region
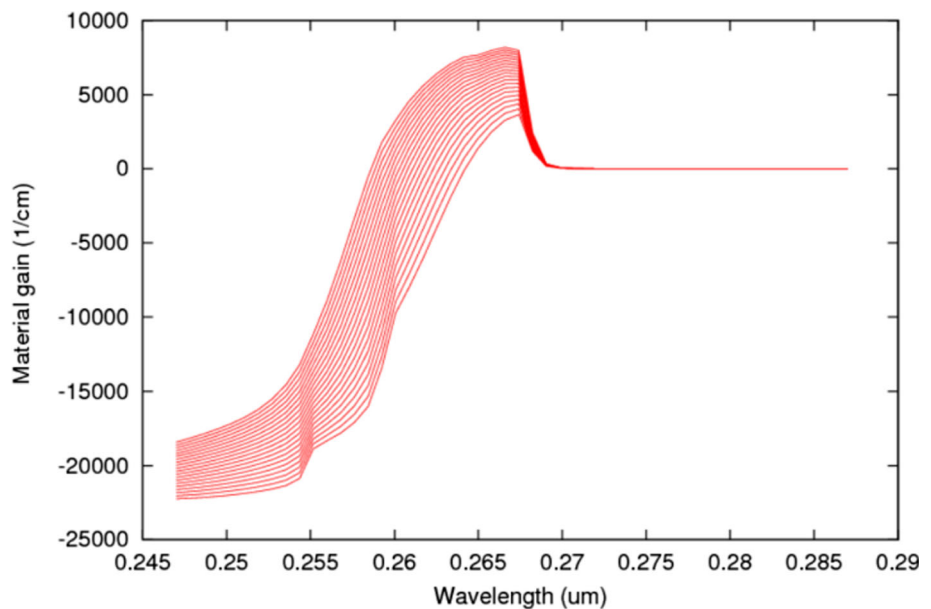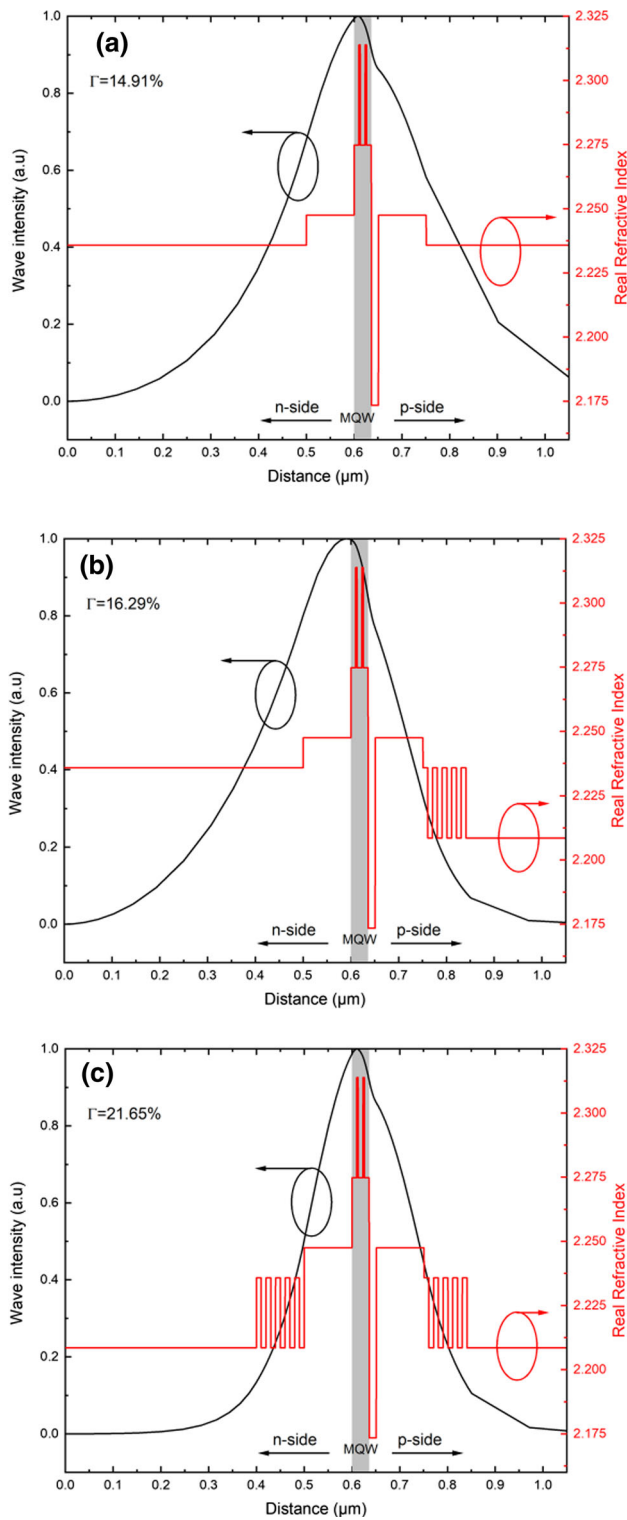
Fig. 3 The real refractive index profiles and near field optical model profiles for LDs with **a** LD1 ($\Gamma = 14.91\%$), **b** LD2 ($\Gamma = 16.29\%$) and **c** LD3 ($\Gamma = 21.65\%$). The horizontal scale indicates the distribution position of each layer of the optical field

waveguide layer (n-WG), two-period of multiple quantum well (MQW) ($Al_{0.58}Ga_{0.42}$ N/$Al_{0.68}Ga_{0.32}$ N), Al-rich 15 nm $Al_{0.94}Ga_{0.06}$ N Electron blocking layer (EBL), 0.1 μm Mg-doped $Al_{0.75}Ga_{0.25}$ N waveguide layer (p-WG) and 0.5 μm Mg-doped $Al_{0.78}Ga_{0.22}$ N cladding layer (p-CL). The thickness of quantum well and quantum barrier is 3 nm and 10 nm, respectively. The Si doping concentration for n-type and Mg doping concentration for p-type layers are fixed, which are 3×10^{19} cm^{-3} and 5×10^{19} cm^{-3}, respectively. The LD structure design is based on AlGaN UV LD on SiC proposed by Sun et al. [19]. There are two other modified structures (LD2 and LD3). In the LD2 structure, the p-CL region in LD1 is replaced with a superlattice structure of 5 period p-$Al_{0.78}Ga_{0.22}$N(0.01 μm)/p-$Al0.85Ga_{0.15}$N(0.01 μm) and 0.4 μm thick p-$Al0.85Ga_{0.15}$ N part. LD2 and LD3 share the same p-CL region, and the n-CL region of LD3 consists of 5 period n-$Al_{0.78}Ga_{0.22}$ N (0.01 μm)/n-$Al0.85Ga_{0.15}$N (0.01 μm) and 0.4 μm thick n-$Al0.85Ga_{0.15}$N region, The Al composition in the n and p regions are symmetric. All parameters of the three structures remain the same except for the cladding layers. The application of five-period superlattice materials in other layers of DUV light sources has been reported by Ramit et al. to improve the carrier distribution to enhance the performance of DUV light sources [20, 21].

PIC3D (Crosslight Software. Inc) was used to simulate the optical and electrical properties of the DUV LED structure [22]. The Landsberg model MQW gain at 267 nm emission wavelength is derived by calculating the Al composition in the active region, as shown in Fig. 2, which confirms that there are no recombination centers except for quantum wells. It is worth mentioning that the emission wavelength can be tuned by the size and composition of the quantum well [23]. In this simulation, the laser has a width of 4 μm, and both n-type and p-type electrodes are considered ideal ohmic contact. The cavity length is 540 μm. Left and right mirror reflectivity is 30%. The background is 2400. The simulation environment is set to room temperature. At the same time, we also assume that 40% of the polarization charge in the interface is blocked [24–29].

3 Results and discussion

To illustrate the effect of novel cladding layers on the optical properties of DUV LD, the near-field optical model profiles were calculated by numerical simulations. We calculated the physical quantity Γ (optical confinement factor) of the active region for three different structures,

$$\Gamma = \int_{\frac{d}{2}}^{\frac{d}{2}} \varphi^2(x,y)\mathrm{d}x \Big/ \int_{-\infty}^{\infty} \varphi^2(x,y)\mathrm{d}x. \qquad (1)$$
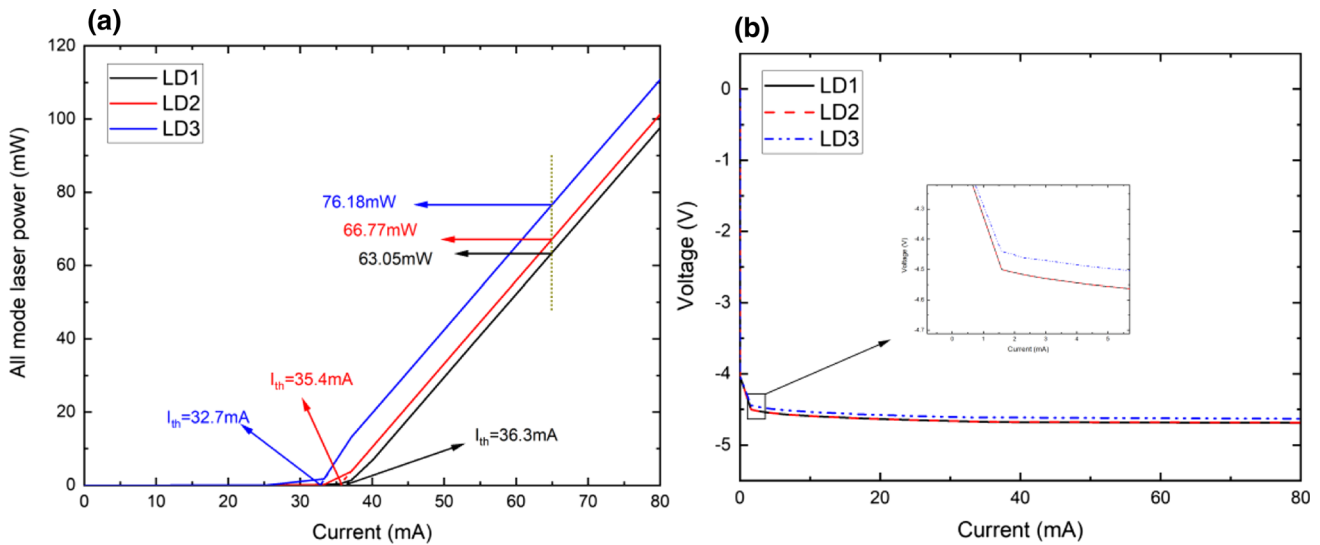
Fig. 4 a Numerically calculated all mode laser power in terms of injection current. **b** Voltage as a function of injection current for three different structures, where the insert the graph showing where the scaled I-V curve section is

where d is the width of the active region and $\varphi(x, y)$ is the wave intensity [30]. The contrast between the real refractive index of the semiconductor and the concentration of electrons and hole carriers in the active region affect the optical gain. The real refractive index distribution and the near-field optical model profiles can be seen in Fig. 3. Among them, LD3 has a high Γ value of 21.65%. The Γ of the structure increases with introducing the new cladding layer, and the Γ of LD2 and LD3 are 1.09 and 1.45 times that of LD1, respectively. These results show that replacing the conventional CL region with novel cladding layers can achieve better optical field confinement in the active region and effectively suppress the optical field leakage from the LD structure. Most of the reported lasers with AlGaN MQW structures have an optical confinement factor of less than 3% [31].

We further explored the effect of the novel cladding layer on the electrical properties of DUV LD. QCSE will reduce the overlap of the electron and hole wave functions and bend the conduction band edges downward, which will adversely affect the output power of the laser. Figure 4a shows the relationship between power and injection current, and the data shows that the threshold current I_{th} for LD3 is the lowest, at 32.7 mA. The corresponding slope efficiency (SE) are 2.26, 2.27, and 2.27, respectively. The slope efficiency of all devices is extracted from the slope of the power and current. When the injection current is 65 mA, the laser output power of LD1, LD2 and LD3 are 76.18 mW, 66.77 mW, and 63.05 mW, respectively. It can be seen from Fig. 4b the $I-V$ curves of the three structures are basically the same, but the threshold voltage of LD3 is the lowest at 4.42 V. The high output power of LD3 at lower threshold currents and voltages proves that the simultaneous introduction of new cladding layers on both sides can provide better electrical characteristics for DUV LD.
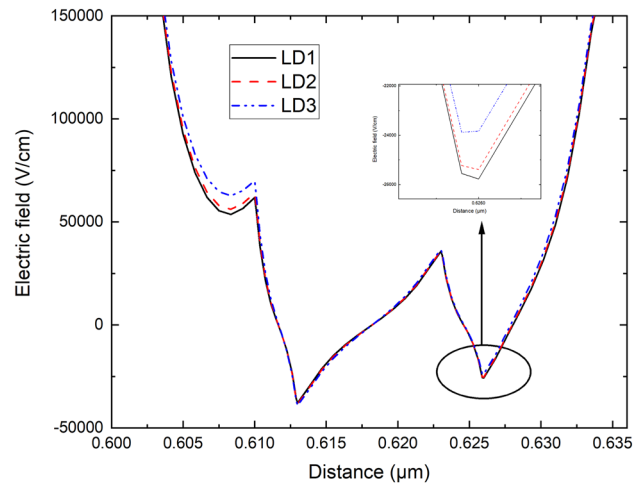
Fig. 5 Internal electric fields of LD1, LD2, and LD3. The higher internal electric field in the MQW adversely affects the performance of the DUV LD, the inset represents the scaled electric field section. Higher electric field in the MQW region can adversely affect the performance of the DUV LD

To identify the above phenomenon, we have studied the internal electric field caused by polarization in the MQW region during laser operation, as shown in Fig. 5. Among the three cladding structures, the electric field inside the quantum well near the p-side of LD3 is the smallest. Specifically, the internal electric fields of LD1, LD2, and LD3 are 25,772, 25,387, and 23,837 V cm^{-1}, respectively. Thus, with the introduction of the cladding layer containing the superlattice structure, the polarization field of the quantum well near the p-side layer is reduced, which leads to a more minor bending of the second quantum well in LD3 due to polarization charge induction and a valence band edge closer to the hole Fermi level, thus increasing the
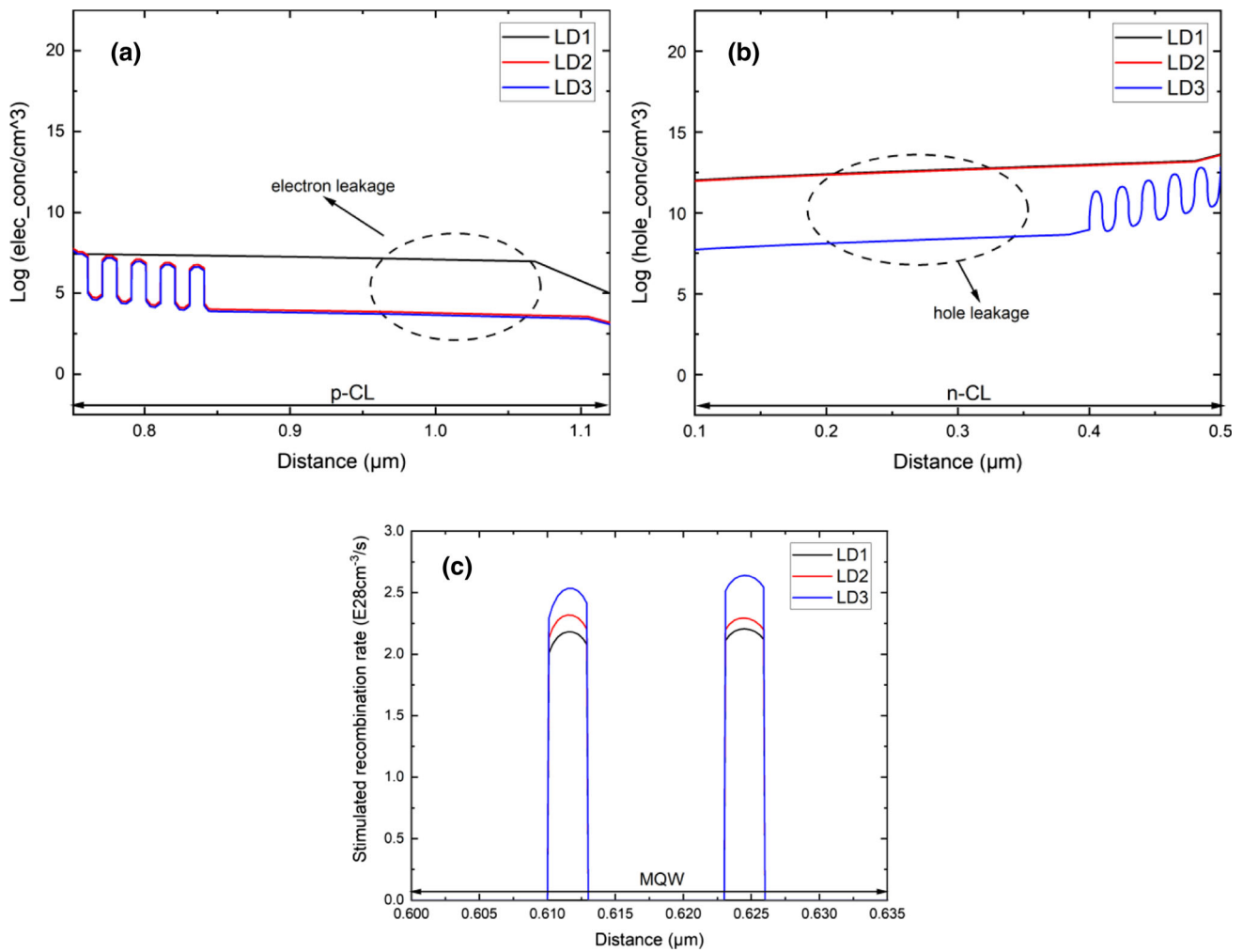
Fig. 6 a Electron concentration distributions in the p-Cl region. **b** Hole distributions in the n-Cl region. **c** Stimulated recombination rate in the MQW region

Table 1 Summary of calculated characteristics for LD1, LD2, and LD3

| DUV LD names	OCF (%)	I_{th} (mA)	S.E(W/A)	Stimulated recombination rate (E28 cm^{-3}/s)
LD1	14.91	36.3	2.26	2.08
LD2	16.29	35.4	2.27	2.19
LD3	21.65	32.4	2.27	2.45

hole injection efficiency and improving the carrier distribution.

Figure 6a illustrates the calculated electron concentration distribution in the p-CL region. A large lattice mismatch induced polarization electric field will attracts large electron concentration at the last barrier/EBL heterogeneous interface, and large electron concentration at the last barrier/EBL interface will result in a lower effective barrier height for electrons, leading to poor electron confinement in the MQW region. We can assess the extent of electron leakage by observing the electron concentration in the p-CL region. Electrons leaking in the p-region force holes to recombine non-radiatively in the p-region before entering the

multiple quantum well region, and LD3 effectively confines electrons to the multiple quantum well region. Similarly, it can be seen from Fig. 6b that the n-region hole leakage of LD3 is minimal, so the injected holes can have a greater chance of compounding in the MQW region. As shown in Fig. 6c, The stimulated recombination rate is significantly increased in LD3 due to the new cladding structure in the n and p regions, which well suppresses carrier leakage and improves the utilization of electrons and holes moreover providing better overlapping of electron–hole wave functions. Thus, an excellent stimulated recombination rate ensures low threshold current, voltage, high output power, and high optical confinement factor.
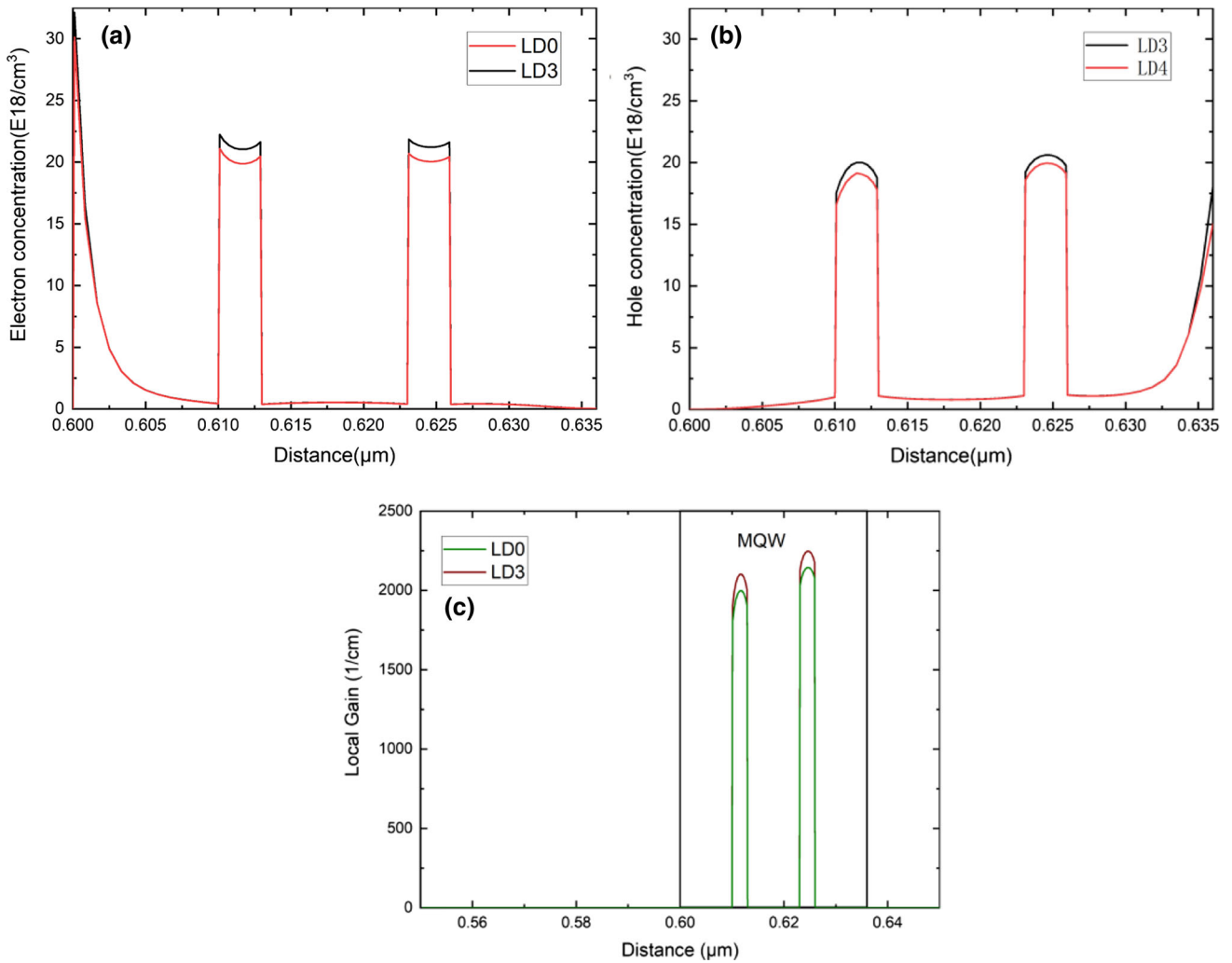
Fig. 7 Numerically calculated **a** electron distribution profiles in MQW, **b** hole distribution profiles in MQW, **c** Local optical gain in MQW at calculated carrier density for LD0 and LD3 respectively, LD3 provides a high gain value for active medium
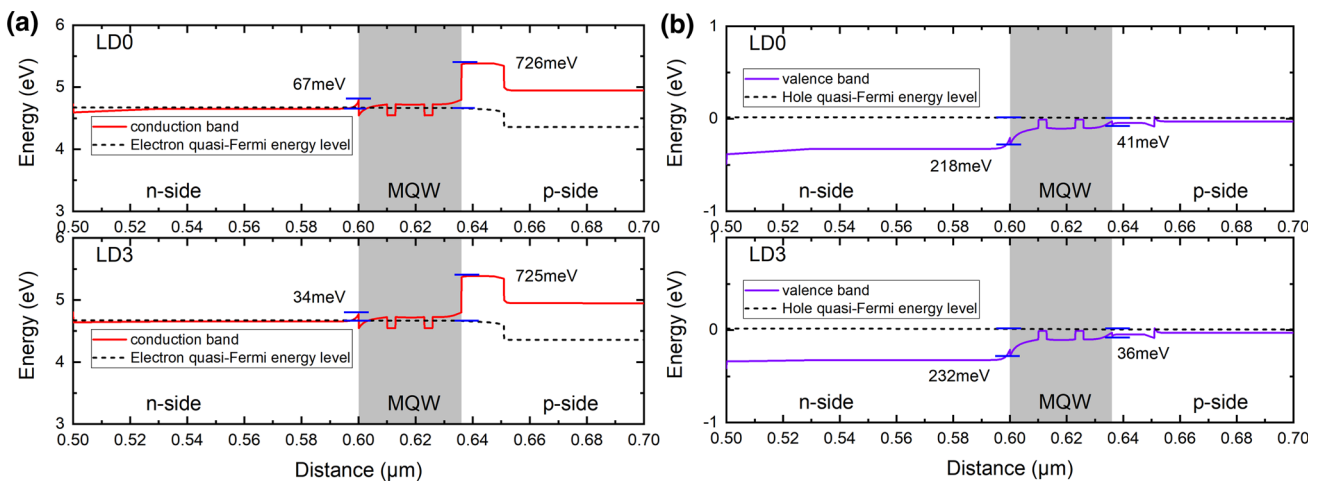
Fig. 8 a Conduction band and Electron quasi-Fermi energy level. **b** Valence band and Hole quasi-Fermi energy level

To compare and illustrate which cladding structure contributes more to the DUV LD performance, Table 1 summarizes the calculated characteristics of the three different LDs.

To further investigate the effect of superlattice cladding on LD, LD0 with the same high refractive index and high potential barrier is added as the reference structure (n-CL for n-$Al_{0.85}Ga_{0.15}N$ and p-CL for p-$Al_{0.85}Ga_{0.15}N$). We calculated the electron distribution as shown in Fig. 7a and can see that the electron concentration of LD3 is higher in the quantum well than in LD0. Figure 7b demonstrates the increase in the hole concentration of LD3 in the MQW region. Figure 7c shows the variation of the local optical gain of the LD due to the interband transitions with distance. We consider all sub-bands that can perform interband transition, and the gain can be changed by the change of the cladding layers. LD3 has a higher local optical gain due to the elevated electron and hole concentrations, suggesting that the superlattice cladding supports better interband transitions. The observation of Fig. 7 can be explained by analyzing the energy band diagram of Fig. 8. If we compare the effective conduction band barrier heights (ECBBH) of LD0 and LD3 in Fig. 8a, we find that LD3 has a lower barrier (34 meV) near the n-side compared to LD0. The lower the potential barrier near the n-side, the higher the chance of electrons flowing into the MQW region, so LD3 has a more efficient electron injection efficiency. LD0 and LD3 have similar potential barriers near the p-side, their ability to hinder electron leakage is comparable. This explains the higher electron concentration of LD3. The presence of EBL suppresses the electron leakage while weakening the hole injection. The effective valence band barrier height (EVBBH) near the p-side affects the hole injection. In Fig. 8b, the lower barrier height near the n-side of LD3 means that holes can flow into the MQW region more easily. Meanwhile, the higher barrier height of LD3 near the n-side effectively suppresses the hole leakage. The above results show that the superlattice cladding layers better improves the energy band bending caused by the polarization electric field, which will optimize the luminescence performance of DUV LD.

4 Conclusion

In conclusion, an AlGaN-based high-efficiency deep-ultraviolet laser diode has been reported. This DUV LD uses a new cladding layer containing a superlattice structure in the n and p regions instead of the conventional AlGaN with fixed Al components. This structure (LD3) not only provides better performance than the conventional structure (LD1), but also has superiority over the structure that optimizes only the p-region (LD2). It is found that the optical confinement factor of the improved structure was significantly increased compared to LD1 (16.29% and 21.65% for LD2 and LD3, respectively). Compared to LD1, the threshold currents of LD2 and LD3 are reduced by 2.47% and

10.74%, respectively, and in addition, the slope efficiency is improved. LD3 has the highest stimulated recombination rate and its superlattice cladding layers create resonator that provides effective confinement of optical fields and carriers. It is believed that the characteristics of LD3 with new cladding layers will help develop optical resonator with better performance for practical applications.

Author contribution

YX: Conceptualization, Methodology, Software, Investigation, Writing—original draft, Writing—review and editing. PZ: Software, Writing—review and editing, Validation. AZ: Software, Resources. MY: Investigation, Validation. FW: Supervision, Project administration, Funding acquisition. JJL: Supervision, Project administration. YL: Supervision, Project administration, Funding acquisition, Writing—review and editing, Validation, Resources.

Data Availability Statements This manuscript has no associated data or the data will not be deposited. [Authors' comment: The datasets generated during and/or analysed during the current study are available from the corresponding author on reasonable request].

References

1. Y. Saito et al., Jpn. J. Appl. Phys. **60**, 080501 (2021)
2. L.M. Hinds et al., Innov. Food Sci. Emerg. Technol. **56**, 102153 (2019)
3. J.L. Lyons et al., Phys. Status Solidi (b) **252**, 900 (2015)
4. G. Matafonova, V. Batoev, Water. Res. **132**, 177 (2018)
5. M. Buonanno et al., Sci. Rep. **10**, 10285 (2020)
6. K. Sato, S. Yasue, Y. Ogino et al., Phys. Status Solidi **217**, 1900864 (2020)
7. M.A. Khan et al., ACS. Appl. Electron. Mater. **2**, 1892 (2020)
8. J.H. Park et al., ACS Energy Lett. **3**, 655 (2018)
9. K.B. Nam, Appl. Phys. Lett. **83**, 878 (2003)
10. A. Khan, K. Balakrishnan, T. Katona, Nat. Photonics **2**, 77 (2008)
11. Z. Liu et al., Semicond. Sci. Technol. **35**, 075021 (2020)
12. Z.Q. Xing, Y.J. Zhou, Y.H. Liu et al., Chin. Phys. Lett. **37**, 027302 (2020)
13. Z. Zhang et al., Appl. Phys. Express **12**, 124003 (2019)
14. F. Liang, Superlattices Microst. **132**, 106153 (2019)
15. T. Omori et al., Appl. Phys. Express **13**, 071008 (2020)
16. X. Fan, H. Sun, X. Li, H. Sun, C. Zhang, Superlattices Microstruct. **88**, 467 (2015)

17. B. So, J. Kim, E. Shin, T. Kwak, T. Kim, O. Nam, Phys. Status Solidi **215**, 1700677 (2018)
18. P. Qin, W.D. Song, W.X. Hu, Y.W. Zhang, C.Z. Zhang, R.P. Wang, L.L. Zhao, C. Xia, S.Y. Yuan, Y. Yin, S.T. Li, S.C. Su, Chin. Phys. B. **25**, 088505 (2016)
19. H. Sun, J. Woodward, J. Yin, A. Moldawer, E.F. Pecora, A.Y. Nikiforov, L. Dal Negro, R. Paiella, K. Ludwig Jr., D.J. Smith, T.D. Moustakas, J. Vac. Sci. Technol. B. **31**, 03C117 (2013)
20. R.K. Mondal, V. Chatterjee, S. Pal, Opt. Mater. **104**, 109845 (2020)
21. Y.A. Yin, N. Wang, S.. Li. Li et al., Appl. Phys. A **119**, 41–44 (2015)
22. L. Xiang, D.G. Zhao, H. Yang, J. Semiconduct. **36**, 074009 (2015)
23. M. Yamada et al., IEEE J. Quantum Electron. **21**, 640 (1985)
24. W. Tian, Z.H. Feng, B. Liu, H. Xiong, J.B. Zhang, J.N. Dai, S.J. Cai, C.Q. Chen, Opt. Quant. Electron. **45**, 381 (2013)
25. K. Kojima, Y. Nagasawa, A. Hirano, M. Ippommatsu, Y. Honda, H. Amano, I. Akasaki, S.F. Chichibu, Appl. Phys. Lett. **114**, 011102 (2019)
26. H. Lu, K.X. Dong, D.J. Chen, B. Liu, Appl. Phys. Lett. **100**, 2390 (2012)
27. Y. Wang et al., Chin. Phys. Lett. **36**, 057301 (2019)
28. T. Yan, J. Li, J. Zhang, M. Li, X. Hu, Superlattices Microstruct. **109**, 117 (2017)
29. S.M. Nawaz et al., Superlattices Microstruct. **145**, 106643 (2020)
30. M. Kneissl, T.Y. Seong, J. Han, H. Amano, Nat. Photonics **13**, 233 (2019)
31. S. Tanaka et al., Appl. Phys. Lett. **118**, 163504 (2021)